**Prediction of Human Hand Motions based on Surface Electromyography**

Anqi Wang

Thesis submitted to the faculty of the Virginia Polytechnic Institute and State University in partial fulfillment of the requirements for the degree of

Master of Science

In

Industrial and Systems Engineering

Ran Jin, Chair

Maury A. Nussbaum, Member

Kimberly P. Ellis, Member

May 10, 2017

Blacksburg, Virginia

Keywords: biomechanical simulation, data fusion, motion tracking, support vector regression, surface electromyography

**Prediction of Human Hand Motions based on Surface Electromyography**

Anqi Wang

## ABSTRACT

Tracking human hand motions has raised more attention due to the recent advancements of virtual reality (Rheingold, 1991) and prosthesis control (Antfolk *et al*., 2010). Surface electromyography (sEMG) has been the predominant method for sensing electrical activity in biomechanical studies, and has also been applied to motion tracking in recent years. While most studies focus on the classification of human hand motions within a predefined motion set, the prediction of continuous finger joint angles and wrist angles remains a challenging endeavor. In this research, a biomechanical knowledge-driven data fusion strategy is proposed to predict finger joint angles and wrist angles. This strategy combines time series data of sEMG signals and simulated muscle features, which can be extracted from a biomechanical model available in OpenSim (Delp *et al.*, 2007). A support vector regression (SVR) model is used to firstly predict muscle features from sEMG signals and then to predict joint angles from the estimated muscle features. A set of motion data containing 10 types of motions from 12 participants was collected from an institutional review board approved experiment. A hypothesis was tested to validate whether adding the simulated muscle features would significantly improve the prediction performance. The study indicates that the biomechanical knowledge-driven data fusion strategy will improve the prediction of new types of human hand motions. The results indicate that the proposed strategy significantly outperforms the benchmark date-driven model especially when the users were performing unknown types of motions from the model training stage. The proposed model provides a possible approach to integrate the simulation models and data-driven models in human factors and ergonomics.

**Prediction of Human Hand Motions based on Surface Electromyography**

Anqi Wang

## GENERAL AUDIENCE ABSTRACT

Hand motion tracking is a promising technique for the development of virtual reality and prosthesis. Identifying hand motions based on sensor data is the fundamental step to realize motion tracking. Among all the tracking techniques, surface electromyography (sEMG) is a type of electrical signals that has been proven useful in predicting hand motions in recent years, since sEMG signals can directly reflect muscle activities, and hand motions are controlled by muscle groups. While most studies focus on the classification of human hand motions within a predefined motion set, the prediction of continuous finger joint angles and wrist angles remains a challenging endeavor. In this research, a biomechanical knowledge-driven data fusion strategy was proposed to predict finger joint angles and wrist angles. More specifically, this strategy combined a statistical model with a biomechanical simulation model, and a hypothesis was tested to validate whether adding the biomechanical simulation model would significantly improve the prediction performance. A set of sEMG signals containing 10 types of motions from 12 participants was collected from an institutional review board approved experiment, in order to test the proposed strategy. The results indicate that the proposed strategy significantly outperforms the benchmark statistical models especially when users were performing unknown types of motions from the model training stage. The proposed strategy provides a possible approach to integrate the simulation models and data-driven models in human factors and ergonomics.

## ACKNOWLEDGEMENTS

I would like to thank my advisor Dr. Ran Jin and committee members Dr. Maury Nussbaum and Dr. Kimberly Ellis for their advice. They provided valuable guidance to my research. Special thanks to my advisor Dr. Jin for his great inspiration and encouragement. Appreciation also goes to my lab mates and the members of Occupational Ergonomics and Biomechanics (OEB) Laboratories for their time and efforts. Special thanks to Dr. Sunwook Kim, Mr. Xiaoyu Chen, Mr. Qing Lan and Ms. Kyndal Stakes for their assistances during the experiment and data analysis.

Special thanks to my parents for their unconditional support of my Master education. I cannot finish this research without their patience and love. They have always been supportive of my decision.

**TABLE OF CONTENTS**

## LIST OF FIGURES

## LIST OF TABLES

# CHAPTER 1
# INTRODUCTION

Tracking human body motion, also known as motion capture or posture estimation, is a method to estimate the postures of a human body as the position and configuration change over time (Yan *et al.,* 2010). In particular, hand motion tracking methodologies are able to provide position information of joints and finger segments. These motion tracking methods have been widely applied to fields, such as the translation of sign language (Wu *et al.,* 2015), virtual reality (Rheingold, 1991), prosthesis control (Antfolk *et al.,* 2010) and rehabilitation (Al-Timemy *et al.,* 2013).

Based on the tracking devices, tracking methods can be divided into the following categories: vision based and non-vision based tracking (Zhou et al., 2008). In vision based tracking, optical sensors are often used to collect video data or marker locations as the quantification of human motions. This type of tracking methods can capture motions with high accuracy. However, vision based tracking methods suffer from occlusion problems and their performances highly depend on the illumination conditions (Reis *et al.,* 2015). This study focuses on the non-vision based tracking methods which can be potentially applied to scenarios without illumination or vision.

Typical non-vision based sensors, such as inertial sensors and surface electromyography (sEMG) sensors (see Table 1), have been used to track hand motions in human computer interactions (HCI) and rehabilitation usages. Among the sensor alternatives, inertial and sEMG sensors are two dominant methods for non-vision based tracking (Zhou *et al.,* 2008). Other sensors, such as magnetic and ultrasonic sensors, were also reported in motion tracking researches. However, the inertial sensors are not able to track the position and angles correctly due to the fluctuation of offsets, and measurement noise, hence leading to integration drift. On the other hand, due to the lack of tracking accuracy, typically, magnetic and ultrasonic sensors were jointly used with other sensors techniques.

**Table 1. Non-vision based sensors in motion tracking.**

| Type of sensors | Advantages | Disadvantages |
|---|---|---|
| Inertial | High sensitivity and large capture volume | Unable to determine the position and angle due to the drift problem |
| Magnetic | High sampling rate, small size | Sensitive to ferromagnetic materials |
| Ultrasonic | Can track muscle contraction via cross-sectional imaging | Subject to reflections and occlusions |
| Surface electromyography (sEMG) | Can track muscle contraction | Low signal-to-noise ratio |

sEMG sensors are adopted in our study for the tracking of hand motions due to their effectiveness in the classification of hand motions shown (Al-Timemy *et al.,* 2013; Xing *et al.,* 2014) and their potential usages in scenarios with poor illuminations. sEMG is an electro-diagnostic medicine technique for evaluating and recording the electrical activities produced by skeletal muscles (Robertson *et al.,* 2013). A previous study showed that there was a measureable correlation between human hand motions and sEMG signals (Tenore *et al.,* 2007). Meanwhile, sEMG signals are collected by non-invasive wearable sensors, which are harmless to human body. Moreover, the sEMG sensors are available at much lower prices compared with vision based tracking sensors.

Most of the current studies address the tracking of human hands as a classification problem (Nazmi *et al.,* 2016), where a motion can be classified into a list of predefined motion types. Data-driven models, such as artificial neural network (ANN) (Murata *et al.,* 1994), are used to correlate sEMG signals with motion types directly. In data-driven studies, Time domain (TD) features and wavelet features are typically used as features of sEMG signals. Although the classification accuracy may be satisfactory for data-driven models (e.g., >96%. Adewuyi *et al.,* 2016), most of these models are not able to classify a new motion type which has not been used in training stage. Meanwhile, the accuracy of the

classification is completely based on the similarity of different motion types. It is likely such a classification error will significantly increase when different types of motions become similar.

This study formulates the hand motion tracking problem as a regression problem with continuous responses (i.e., joint angles of index finger and thumb). As a result, these angles can be used to define a new motion type, quantify the variability of motions, and evaluate the similarity of motions in a quantitative way. To predict the joint angles, we integrated biomechanical domain knowledge with statistical modeling steps by adding simulated muscle features (e.g., fiber length, tendon length, tendon force, active fiber force, passive fiber force). Figure 1 provides an overview of this proposed approach.

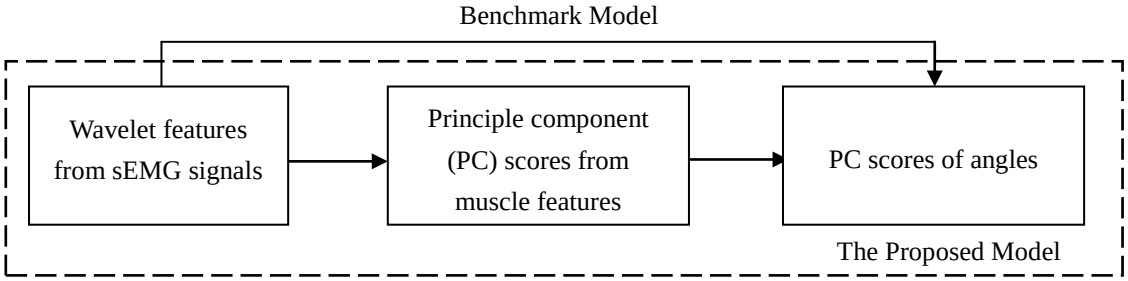


**Figure 1. Modeling stages for the benchmark and proposed models (each arrow represents a regression model).**

In this study, the investigators measured sEMG signals. The muscle features, such as muscle fiber length and muscle-tendon force, were simulated by using the marker coordinates as input variables. The simulation was based on the upper extremity model (Holzbaur *et al.*, 2005) which allowed users to simulate muscle features based on a hand motion defined by joint angles. The simulation was conducted on OpenSim (Delp *et al.*, 2007). Given the muscle features, the investigators proposed a two-stage method, where the wavelet features extracted from sEMG signals were used to predict muscle features in the first stage, and the predicted muscle features were used as predictors to predict joint angles at the second stage.

Muscle features were expected to improve the prediction performance and to provide accurate predictions for new motion types other than the predefined ones in model training step. The proposed strategy is different from the existing data-driven prediction methods,

which typically model the relationship between the sEMG signals and the motion types without biomechanical knowledge based simulation. By incorporating biomechanical knowledge (muscle features), we tested the hypothesis whether adding the simulated muscle features would significantly improve the prediction performance. In this study, ten types of motions were defined and a total of 1200 observations from 12 subjects were collected from an institutional review board (IRB) approved experiment.

The remainder of this thesis is organized as follows. Chapter 2 reviews the literature of motion tracking methodologies, existing models and feature extraction strategies for sEMG signals, and biomechanical simulations. Chapter 3 introduces the experimental design. Chapter 4 shows the data preprocessing, modeling and prediction results. Chapter 5 discusses the results, robustness, limitations and draws the conclusions and future works.

# CHAPTER 2
# LITERATURE REVIEW

## 2.1 Motion Tracking Methods

This section summarizes the state-of-the-art in vision based and non-vision based motion tracking methodologies. In term of the data processing method, vision based tracking can be divided into appearance based and model based tracking (Erol *et al.,* 2005). In the appearance based approach, image features, such as textures and contours, serve as measurements to quantify a motion. The model based approaches assume prior models, such as kinematic model and hand shape model, to fit the data (Lu *et al.,* 2014). Both of these two methods follow a general modeling flow from feature extraction to feature selection and model estimation. The essential difference between appearance based and model based tracking is whether a model is used to fit the data.

Different than vision based tracking, non-vision based tracking systems use non-optical sensors to record human motions in the form of electrical signals (Ueda *et al.,* 2016). Non-vision based tracking methods have been commonly used because they do not suffer from occlusions (Zhou *et al.,* 2008). Inertial sensors (e.g., accelerometer and gyroscope), magnetic sensors, and ultrasonic sensors have been applied to the tracking of the human hands in research studies. Inertial sensor based tracking system (Zhou *et al.,* 2006) have been well studied during the last two decades because of their high sensitivities and abilities to track motions in a large capture volume (Najafi *et al.,* 2003; Lyons *et al.,* 2005). However, inertial sensors suffer from drift problem and the design of sensor placement need to be customized case by case based on kinematic principles. Magnetic sensors form another type of track sensors with small sizes, high sampling rates, but large jitters and high latencies. Noort *et al.* (2016) developed a measurement system using the combination of inertial and magnetic sensors in order to track finger movements. Ma *et al.* (2011) designed a wireless magnetic hand motion tracking systems using small magnets placed on the finger tips. Both of inertial sensors and magnetic sensors need to be placed on human hands, which add external loads to human hand and will restrict hand movements. Other sensors, such as ultrasonic sensor (Akhlaghi *et al.,* 2016), bend and force sensors (Simone *et al.,* 2005), were

also reported to be used in tracking human hand motions.

sEMG has been the predominant method for sensing electrical activity in ergonomic and biomechanical studies with applications to prostheses control and rehabilitation (US Department of Public Health Service, 1992). In recent years, researchers have shown an increasing interest of studying sEMG signals in the field of motion tracking, due to the development of wearable sensor technologies and machine learning algorithms. Different from inertial sensors and magnetic sensors, sEMG sensors can be placed at the external areas of the hand (e.g., on the forearm) while still maintain a desirable tracking accuracy (Adewuyi *et al.*, 2016). The reason is that hand external muscles play vital roles in the control of hand motions (Tyldesley *et al.*, 1989). And sEMG signals can represent the activity in individual muscle or muscle groups over which the electrodes are placed.

The generation of muscle activities is a complicated process which involves the interaction of nerves, bones, and muscle fibers. Therefore, the signals collected from the surface of human skin could be noisy and have unwanted contributions from the environment. In order to find useful information out of the noisy sEMG signals, feature extraction methods are commonly used.

### 2.2 Feature Extraction and Modeling Methods for sEMG Signals

Many studies have been conducted in discriminate hand motions using sEMG signals. Table 2 provides a summary of the feature extraction methods in the classification of human hand motions using sEMG signals.

**Table 2. Summary of literature review.**

| Title | Feature Extraction | Authors | Motions |
|---|---|---|---|
| Recognize Finger Motions Using Wavelet Transform | Wavelet Transform | Jiang *et al.*, (2006) | Flexion-extension of thumb, index, middle fingers separately |
| Identify Low Level Muscle Activities Using Fractal Dimension Features | Independent Component Analysis (ICA) | Naik *et al.*, (2009) | Four finger group movements |
| Decode Individuated Finger Movements Using sEMG | TD features | Tenore *et al.*, (2009) | Flexion-extension for individual fingers and finger group movements |
| Decode Individuated Finger Movements Using Genetic Algorithm | TD features | Kanitz *et al.*, (2011) | Individual finger movements |
| Analysis of Intrinsic and Extrinsic Hand Muscle EMG for Improved Pattern Recognition Control | TD features | Adewuyi *et al.*, (2016) | Online study on wrist movements |
| Orthogonal Fuzzy Neighborhood Discriminant Analysis for Myoelectric Hand Control | A combination of TD and AR features | Khushaba *et al.*, (2010) | Forearm and wrist movements |

Note: TD refers to time domain feature extraction. LDA refers to linear discriminant analysis. ICA refers to independent component analysis. AR refers to autoregressive features.

TD features, such as wave length (WL) and mean absolute value slop (MAVS), have been adopted in the classification of hand motions, because of their easy accessibility and low computational costs. For example, Adewuyi *et al.* (2016) designed three types of finger motions in seven different wrist positions. They analyzed the sEMG data extracted from

amputees using TD features and linear discriminant analysis (LDA). The classification accuracy can reach up to 96% for amputees; Tenore *et al.* (2009) also applied traditional TD features, such as Willison amplitude (Zardoshti-Kermani *et al.,* 1995), in order to decode the flexion and extension motions of individual fingers.

Although TD features are popular in sEMG studies due to their low computational costs and desirable accuracy in classification studies, the stability of TD features was affected by sensor shifts. A study showed that the unstable TD features would cause a significant reduction in accuracy (Tkach *et al.,* 2010). Wavelet features may compensate the drawbacks of TD features when the disturbances of sensor shifts affect the sEMG signals on time domain. Because wavelet functions resemble the motor unit action potentials that represent the gross sEMG signals in time-frequency domain (Chu *et al.,* 2006), which could be more robust to the disturbance. A comparison study showed that wavelet features performed better at overcoming the disturbances of electrode shifts compared with TD features (Fontana *et al.,* 2014). A case study has shown that wavelet features are able to classify finger motions with a high discrimination ratio (Jiang *et al.,* 2006).

Other statistical methods have been studied to extract features from sEMG signals. For instance, independent component analysis (ICA) and fractal dimension (FD) have been used to identify low level forearm muscle activities. ICA and FD were used by Naik *et al.* (2009) as the feature selection methods before applying an artificial neural network (ANN) model.

Human hands consist of small anatomical segments with high degree of freedoms (DoFs) (Ishii *et al.,* 2011) that could complicate the motions analysis of human hand. In recent years, many classification algorithms (Nazmi *et al.,* 2016) have been studied to classify different types of human hand motions using sEMG signals. Typical classification algorithms, such as K-nearest neighbors (KNN), LDA, ANN and support vector machines (SVM), have been applied to sEMG analysis. Liu (2014) studied how different classifiers would affect the classification results using LDA, KNN and SVM classifiers.

Apart from the classification studies, a few studies were reported in the prediction of continuous responses (e.g., finger joint angles). ANN has been used by researchers to capture the complex relationship between sEMG signals and finger joint angles. As a nonlinear model, ANN was shown to be capable of estimating continuous finger joint angles in a setting of

periodical flexion-extension finger motions (Shrirao *et al.,* 2009). Ngeo *et al.* (2012) used ANN to fit the input of muscle activation features obtained from sEMG signals. Hioki *et al.* (2012) applied an ANN model with six system parameters and reported the prediction result of 7.1-11.8% root mean square error (RMSE).

### 2.3 Applications of Biomechanical Simulations

Biomechanical simulation is the process of imitating human motions over time by a biomechanical model, which can represent the physical or mathematical relations of different parts of human bodies. Biomechanical simulations can be divided into two types: the inverse dynamics and forward dynamics. The inverse dynamics model computes joint forces and moments from observable kinematic information, such as center of mass, position of markers, velocities and accelerations (Logar *et al.,* 2015). The forward dynamics model sets the variables of motions in response to applied forces or moments (Patton, 1993). These simulations can be applied to surgical planning, sports biomechanical analysis and ergonomics (Ma *et al.,* 2010). OpenSim (Delp *et al.,* 2007) is an open-source simulation software which provides a platform for performing both types of simulations. Its inverse dynamics model can compute a set of body parameters, such as muscle features from the estimated accelerations of an input motion. In contrast to the inverse dynamics, the forward dynamics model describes how motions change in response to input controls and external forces (Seth *et al.,* 2011). The Stanford upper extremity model (Holzbaur *et al.,* 2005) is an inverse dynamics model built upon the OpenSim (Delp *et al.,* 2007) platform, which includes 15 DoFs representing the shoulder, elbow, forearm, wrist, thumb, and index finger, and 50 muscle compartments crossing these joints. This model is able to provide accurate estimations of muscles and joints, and capture important interactions between joints (Gonzalez *et al.,* 1997). However, the simulation is always a representation of the underline physics which means the accuracy of a simulation model depends on the fidelity of the underlying mathematical model (Tsang *et al.,* 2005). Also, the complexity of the interactions between muscles and human motions make it hard to build a generic model that is applicable to all kinds of motions using pure data fusion methods. Therefore, we combined simulation data with the data from the real-world experiment, so that the integrated model should be

more robust and more interpretable than data-driven models.

# CHAPTER 3
# USER STUDY AND DATA REVIEW

## 3.1 Experiment Design

### 3.1.1 Apparatus

As mentioned in Chapter 2, vision based tracking methods may have occlusion problems but can provide tracking results with high accuracy. Therefore, this study used vision based tracking system as the ground truth data to our prediction. In our experiment, two tracking systems were used to record the hand motions: 1) Vicon motion capture system (Vicon Motion Systems, Oxford, England) which provided accurate tracking data as ground truth, and 2) MYO sEMG armband. Details of the devices instrumented are listed in Table 3.

**Table 3. Instrumentation.**

| Device Type | Numbers | Placement | Function |
|---|---|---|---|
| Mocap cameras | 10 | Around the capture volume | Detect marker locations in 3D space (x, y, z) |
| Reflective markers | 20 | On the right hand | To be detected by cameras |
| sEMG armband | 1 | Right forearm | Proved raw sEMG signals |
| Control computers | 1 | On the work bench | Assist optical video data acquisition |
| Laptop | 1 | On the work bench | Control the application for sEMG signal streaming and recording |

### 3.1.2 Participants

A total of twelve right-handed participants with ages varying from 20 to 32 (mean=23.9, stdev=3.68) were recruited from the university population including undergraduate and graduate students in Virginia Tech, among which five were females and seven were males. All of the participants had full capability of their forearm and did not have any self-reported

musculoskeletal disorder or associated pain for at least three months before testing. The information was verified using a background screen questionnaire. The study was approved by Virginia Tech IRB with case number 16-1082.

### 3.1.3 Design of Motions and Marker Placement

Ten motions were collected from the experiment, namely, index finger flexion, index finger extension, thumb flexion, thumb extension, wrist flexion, wrist extension, wrist abduction, wrist adduction, supination and pronation. When performing finger flexion or extension motions, participants were asked to move only metacarpophalangeal (MCP) joints by keeping their fingers stretched and hands still. The standard motions all started from a neutral position and ended at the position of maximum flexion or extension that the participants can reach.

An armband was placed at the proximal end of the participant's forearm. 20 passive reflective markers were also attached to the surface of the participant's right hand using double-sided tape. The design of marker set refers the marker placement in a study tracking musician's hand activities when they are performing piano (Goebl *et al.*, 2013). As presented in Figure 2, the investigators placed 17 of the 3mm markers on each joint of the fingers and on the plane of the hand. For the wrist, we used three of the 6mm markers instead of 3mm markers because 6mm markers flickered less during the calibration process.

**Figure 2. Marker placement.**

### 3.1.4 Experiment Procedures

The experiment involved a training session and a data collection session. In the training session, the investigators explained the motions with the demonstration part of a training video. Next, each participant was instrumented a sEMG armband and 20 markers with the help of an investigator. Afterwards, the participant would follow the practice part of the training video and tried to perform each motion following the instructions till he or she felt comfortable and familiar with the tasks. The training session took about 1-1.5 hours in order to let the participant get familiar with the designed motions.

During the data collection session, the participant was reminded of the predefined motion by one of the investigators, and was required to replicate each one of the 10 predefined motions for 10 times. Between each replication, a 5-second rest was allowed. At the beginning of each recording, the participants were seated in front of a table with half of the right forearm placed on the table as shown in Figure 3. The participant would be asked to remain the forearm at a neutral, comfortable position which was neither supinated nor pronated before the recording. Next, the participant would get a start sign from an investigator to start performing the corresponding task at a slow, constant rate within 3 seconds. Upon finishing, the participant would remain the right hand at the ending position of the movement until the recording period ended.

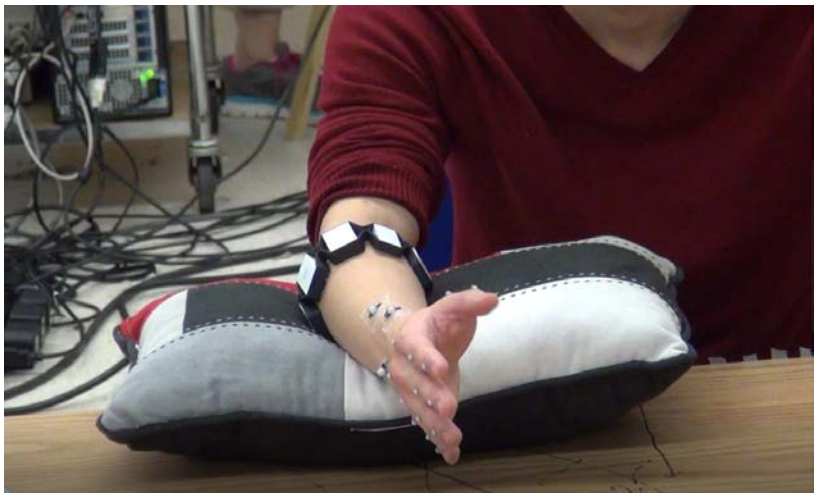

**Figure 3. Neutral position.**

### 3.2 Data Analysis and Simulation

This section provides a review of the data collected from the experiment, including the data from experiment and simulation data collected from the Stanford upper extremity model (Holzbaur *et al.*, 2005) in OpenSim (Delp *et al.*, 2007). The model is a static musculoskeletal model which is able to simulate the corresponding muscle features, such as fiber length, fiber forces and tendon length given a joint angle. Figure 4 shows the data fusion processes, which illustrate how the experiment data are integrated with the simulation. Firstly, two types of raw data, the 3D marker location and sEMG signals, were collected from optical sensors and sEMG sensors respectively. Secondly, joint angles were calculated based on the marker coordinates. Afterwards, the joint angles were input into the OpenSim simulation model, which would output muscle features. The proposed biomechanical knowledge-driven data fusion strategy included two stages (see Figure 4), where the first stage was to use sEMG signals to predict muscle features and the second stage was to build an inverse model to predict joint angles. Therefore, the three data sets that would be used in the model training stage were 1) sEMG signals, 2) muscle features, and 3) joint angles. Table 4 summarizes the data sets and their annotations.

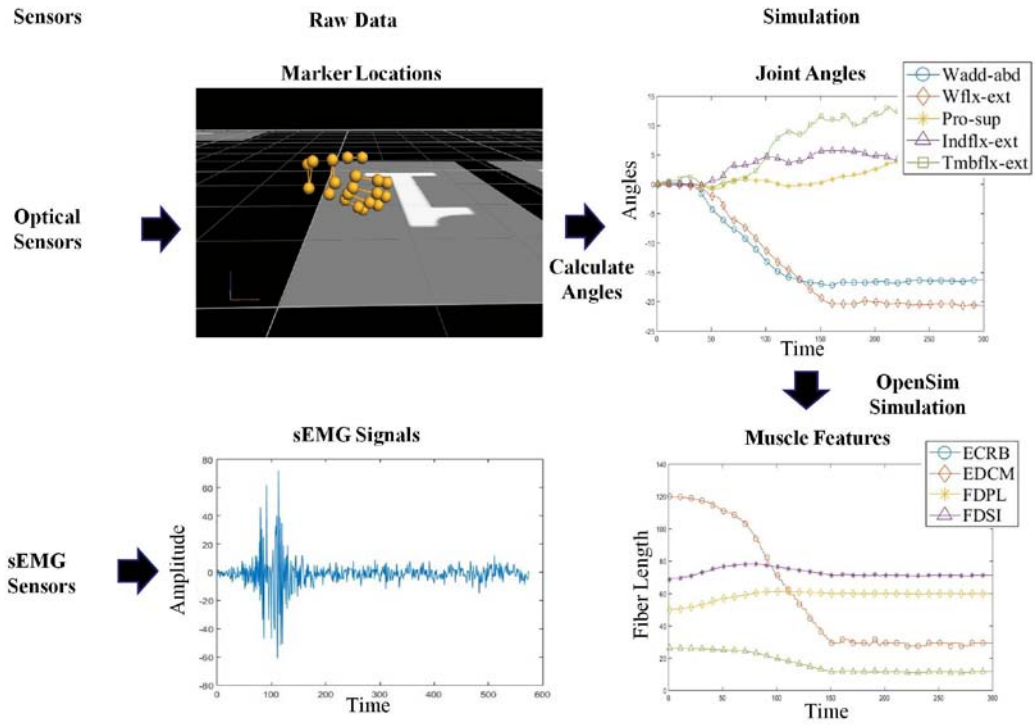


**Figure 4. Data fusion (arrows represent the steps of data acquisition or processing).**

**Table 4. Summary of data sets.**

| Data sets | Annotations |
|---|---|
| sEMG Signals | $X^{(i)}(t)$ represents the amplitude of sEMG signal at channel $i$ at time point $t$, where $i = 1, 2, \dots, 8$. |
| Joint Angles | $Z^{(k)}(t)$ is a matrix with each column representing the change of angles over time. The type of joint angle is denoted as $k$, where $k = 1, 2, \dots, 5$. |
| Muscle Features | $Y^{(h)}(t)$, where $h$ denotes the type of muscle feature, $h = 1, 2, \dots, 60$. |

Accordingly, all of the N observations are denoted as $\boldsymbol{x}_1^{(i)}, \boldsymbol{x}_2^{(i)}, \dots, \boldsymbol{x}_N^{(i)}$ for sEMG signals from channel $i$, $\boldsymbol{y}_1^{(h)}, \boldsymbol{y}_2^{(h)}, \dots, \boldsymbol{y}_N^{(h)}$ for muscle features from muscle feature $h$, and $\boldsymbol{z}_1^{(k)}, \boldsymbol{z}_2^{(k)}, \dots, \boldsymbol{z}_N^{(k)}$ for finger joint angle $k$. The 8-channel sEMG signals were collected at the proximal end of forearm with a sampling frequency of 200 Hz. Each observation contains a 3-second record. The joint angles considered in this study include flexion-extension angles of thumb and index finger, abduction-adduction angles, flexion-extension angles of wrist and pronation-supination angles. Each joint angle was calculated based on the angles between hand segments and surface normal. The details of the calculations for theses angles are in Appendix A. The definitions of the joint angles in the calculations are consistent with those in the OpenSim (Delp *et al.*, 2007) musculoskeletal model, where five dynamic joint angles were related to the pre-defined motions.

Different than the above two types of data which can be collected or calculated from real world experiment, muscle features were exported from OpenSim (Delp *et al.*, 2007). This simulation model includes underlying functions describing the relationship between muscle features and joint angles, which allow the users to export the corresponding muscle features in response to hand motions. The following muscle features are available in the model: 1) fiber length, 2) tendon length, 3) tendon force, 4) active fiber force, and 5) passive fiber force.

Muscle fiber, the unit of structure of a skeletal muscle, is composed of numerous myofibrils that contract when stimulated (Tyldesley *et al.*, 2009). Muscle tendon is a type of tissue that unites muscle fibers to bone. Studies have shown that features, such as muscle fiber length (Arnold *et al.*, 2013), fiber force and tendon force measurements (Gregor *et al.*, 1994) are related to hand movements. Therefore, we integrated muscle features in the modeling process. This model has its underlying functions to project joint angles to muscle features discretely, while muscle features are simulated by matching the simulated joint angles with the closest joint degrees calculated from marker locations.

# CHAPTER 4

# MODELING METHODOLOGY

## 4.1 Data Preprocessing and Feature Extraction

Three steps of data preprocessing methods are applied on the three types of data sets in order to prepare input data for the proposed model: 1) to remove those observations with missing data points, 2) to filter data to remove any unwanted noises in the trajectories, and 3) to extract features in order to reduce the dimension of functional data.

Missing data points due to marker occlusion is a common problem addressed in marker based motion capture (Federolf, 2013). In this study, marker occlusion also caused missing data points in some observations. Although the placement of marker sets was designed to avoid unwanted movement (e.g., soft tissue movement), the chances are that marker flickered from time to time. These imperfections, however, affect model performance because missing values need to be interpolated properly and modeled in a different way. In this study, we only used the complete observations in the modeling process.

### 4.1.1 Processing and Feature Extraction of sEMG Signals

Wavelet transform based denoising and feature extraction methods were used in this study. Because wavelet out performs other methods when processing non-stationary signals whose frequency and magnitude vary with time (i.e., sEMG signals). Therefore, wavelet based filtering method was applied to sEMG signals. The following content describes the steps for denoising. First, the wavelet coefficients were obtained by conducting wavelet decomposition of the sEMG signals. And then the detail wavelet coefficients based on a threshold calculated via Stein's unbiased risk estimation (SURE), which provides an unbiased estimation of the mean squared error for any 1D signal (Donoho *et al.*, 1995). Afterwards, signals were reconstructed back to time domain based on the filtered wavelet coefficients. Similar denoising method has been applied to EMG signals by Sobahi (2011) in his sEMG study.

In order to extract time-frequency feature set, we first decomposed the reconstructed signals into three time windows considering the time effect in different motions. Then

wavelet transformation was performed using Symlet 4 wavelet function (Misiti *et al.*, 1996) within each of the 3 time windows. The Symlet 4 wavelet function was chosen based on the smoothness of the signal. The above procedure repeated for all the 8-channel signals so that wavelet coefficients of all of the 8 channels can be obtained. However, directly using wavelet coefficients as features would result in high dimensionality when comparing with the sample size. Therefore, wavelet energy and standard deviation of each level of the wavelet coefficients were calculated in order to reduce the dimensionality. In the end, for each sample, features (wavelet energies and standard deviations) of 8 channels were concatenated into one vector. Hereby, 192 features (i.e., 8 channels * 3 windows * 4 wave levels * 2 feature types = 192) were extracted to serve as the predictors of the proposed model.

### 4.1.2 Processing of Muscle Features and Angles

For the other two types of functional data which are smoother than sEMG signals (i.e., the joint angles and muscle features), we adopted the multivariate functional principle analysis (MFPCA) proposed by Happ *et al.* (2016) in order to reduce the dimensionality. Their method provided an estimation of the multivariate functional principle components and principle component (PC) scores based on the univariate principle component decomposition for each dimension. The detailed steps of the estimation strategy are described in Appendix B. We selected the first five PCs corresponding to 99% of the total eigen values. Figure 5 shows an example of the reconstruction result of the wrist flexion-extension angle coming from the 10-th replication of wrist extension motion.

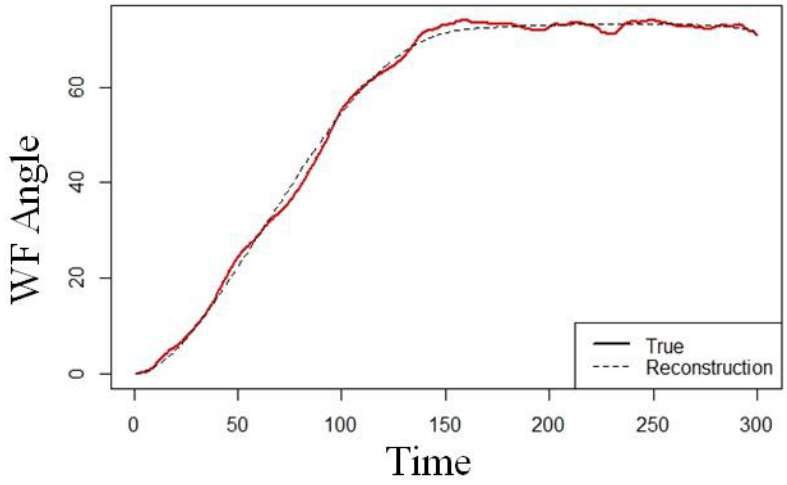


**Figure 5. Reconstructed angles v.s. true angles.**

MFPCA was also applied to the functional muscle features in order to extract PC scores. Hereby, all of the three data sets (sEMG signals, muscle features and joint angles) were represented in their features. The prediction and model training were based upon these feature sets rather than the raw data. Specifically, the sEMG features were used to predict PC scores obtained from muscle features, and the predicted muscle features were used to predict the angles.

### 4.2 Proposed Method

In order to test the hypothesis whether adding the simulated muscle features would significantly improve the prediction performance, we proposed a biomechanical data fusion modeling system which was composed of two stages. As shown in Figure 1, in the first stage, wavelet features extracted from sEMG signals (denote as X) were used to predict PC scores extracted from muscle features ($Y$). At the second stage, the predicted $Y$ was used to predict the PC scores extracted from joint angles (denote as Z). As a comparison of the performance, the benchmark model was set to using X to predict Z directly. Benchmark model and the proposed model used the same type of regression model and the same cross-validation (CV) folds. The only difference was whether muscle features $Y$ were involved in the modeling process. Therefore, their prediction results were comparable to each other.

In order to test the prediction performance of the proposed model when being applied to

a new motion, leave-one-motion-out CV was adopted (Geisser, 1993). Specifically, nine out of ten types of motions were used as training set in turn, and the remaining one type of motions was left out as the testing set of the model. For example, if data of Motion Types 2 to 10 are used as the training data set, then data of Motion Type 1 are used as the testing data set. Stratified CV method was also adopted in the purpose of comparing the robustness of the models. The stratified CV aimed to ensure a balanced number of testing samples for each type of motion in the training and testing sets.

Due to the effectiveness shown in previous studies (Alkan *et al.,* 2012; Alazrai *et al.,* 2016), support vector regression (SVR) with linear kernel was used in the modeling process for both the benchmark and proposed models. SVR adopts the same principles as SVM proposed by Vapnik (2013), which minimizes errors by individualizing hyper-planes to maximize the margin. The basic idea is to find a function that has at most $\varepsilon$ deviation from the true response point $y_n$ for all the training data and at the same time as flat as possible. Different from traditional regression procedures, the loss function of SVR treats the fitting error as zero if the loss is lower than a tolerance value. Only those points outside the tolerance zone will be penalized (Alkan *et al.,* 2012). Specifically, in linear SVR, the generalized error boundaries are the combination of the norm of regression coefficients and a regularization term that controls the complexity of the hypothesis space (Basak *et al.,* 2007) as formulated in Equation (1),

$$min\, J(\boldsymbol{\beta}) = \frac{1}{2}\boldsymbol{\beta}^T\boldsymbol{\beta} + C\sum_{n=1}^{N}(\xi_n + \xi_n^*), \tag{1}$$

where $\boldsymbol{\beta}$ denotes the vector of regression coefficients, $C$ is the cost, $\xi_n$ and $\xi_n^*$ are slack variables for the sample $n$. The objective function subjects to the constraint that the residuals are within the margin $\varepsilon$ for all the samples,

$$y_n - (\boldsymbol{x}_n^T\boldsymbol{\beta} + b) < \varepsilon + \xi_n,\ \forall n, \tag{2}$$

$$(\boldsymbol{x}_n^T\boldsymbol{\beta} + b) - y_n > \varepsilon + \xi_n^*,\ \forall n, \tag{3}$$

$$\xi_n^* > 0,\ \forall n, \tag{4}$$

$$\xi_n > 0,\ \forall n, \tag{5}$$

where $y_n$ is response, $\boldsymbol{x}_n$ represents predictors and $b$ is the intercept. As shown in the Equation (1), the objective function is a combination of the $l^2 - norm$ of regression

coefficient term with a cost function. The constant $C$ determines the trade-off between the flatness of the function and the amount up to which deviations larger than the tolerated zone. In order to find the suitable regression function, we tuned the parameter $C$ and $\varepsilon$ via performing CV over the training data. The proper tuning parameter selection was based on minimum cross validated RMSE. The model parameters are estimated by using dual stochastic gradient descent (SGD) method (Hsieh *et al.*, 2008).

### 4.3 Results

The prediction results are reported in terms of two CV strategies for the benchmark and the proposed models. In order to compare the prediction performance with original observations, we reconstructed the joint angle curves to time domain using the predicted PC scores of joint angles via Equation (6).

$$\hat{Z}_n^{(k)} = \sum_{m=1}^{M} \hat{\rho}_{n,m}\, \hat{\psi}_m^{(k)} + \mu_n^{(k)}, \tag{6}$$

where $\hat{\rho}_{n,m}$ is the estimated $m$-th PC score vector of $n$-th sample; $\hat{\psi}_m^{(k)}$ is the estimated multivariate principle components. Each PC has the same structure as $\hat{Z}_n^{(k)}$, and the mean function $\mu_n^{(k)}$ is from the training set so that the reconstructed function of the joint angle $\hat{Z}_n^{(k)}$ ,where $k = 1,2,\ldots,5$ and $n = 1,2\ldots N$, can be obtained. Hence RMSE value for each sample can be calculated via

$$RMSE_n = \sqrt{\frac{1}{T}\sum_{t=1}^{T}(\hat{Z}_n^{(k)}(t) - \hat{Z}_n^{(k)}(t))^2}. \tag{7}$$

The averaged RMSE given by

$$RMSE = \frac{1}{N}\sum_{n=1}^{N} RMSE_n, \tag{8}$$

and the overall standard error of RMSE via

$$SE = \frac{1}{\sqrt{N}}\sqrt{\frac{1}{N-1}\sum_{n=1}^{N}(RMSE_n - RMSE)^2}. \tag{9}$$

Figure 6 shows the modeling results, i.e., the RMSE (in the unit of degree) of the benchmark and the proposed models for the predicted five joint angles. Each colored bar represents the averaged RMSEs calculated via Equation (8), while the length of the line segments at the top of the bar represents $\pm 1$ times standard error of RMSEs obtained from

Equation (9). Tables A2 and A3 in Appendix C show the corresponding values for each bar. There are two groups of bars in each figure. The left bar groups represent the prediction results for the two models using the 10-fold stratified CV strategy. The 10-fold stratified strategy is to include all types of motions in each fold with equal number of observations for each motion type. The averaged RMSE values for benchmark model are higher for the prediction of the pronation-supination, wrist flexion-extension and index flexion-extension angle but are slightly lower in the prediction of the other two types of angles. The right bar groups denote the results from leave-one-motion-out CV strategy. The leave-one-motion-out refers to the 10-fold CV strategy, where all the replications of the nine motions are used as the training set (90% of the total sample size) while the remaining one type of motion (10% of the sample size) is ruled out as the testing set. The prediction errors (RMSE) for the proposed models are all lower than the benchmarks. Furthermore, the difference between the benchmark model and the proposed one is larger than one standard error for all the angles except the wrist flexion-extension angle. The range of each angle is 80 degrees for wrist abduction-adduction angle, 185 degrees for wrist flexion-extension angle, 158 degrees for pronation-supination angle, 170 degrees for index flexion-extension angle and 102 for thumb flexion-extension angle. The RMSE percentages of the five angles (averaged RMSEs over ranges) were 8.67-9.97% for the benchmark method under stratified CV strategy, 8.49-10.17% for the proposed method under stratified CV strategy, 10.25-11.63% for the benchmark method under leave-one-motion-out CV strategy and 9.11-10.78% for the proposed method under leave-one-motion-out CV strategy.

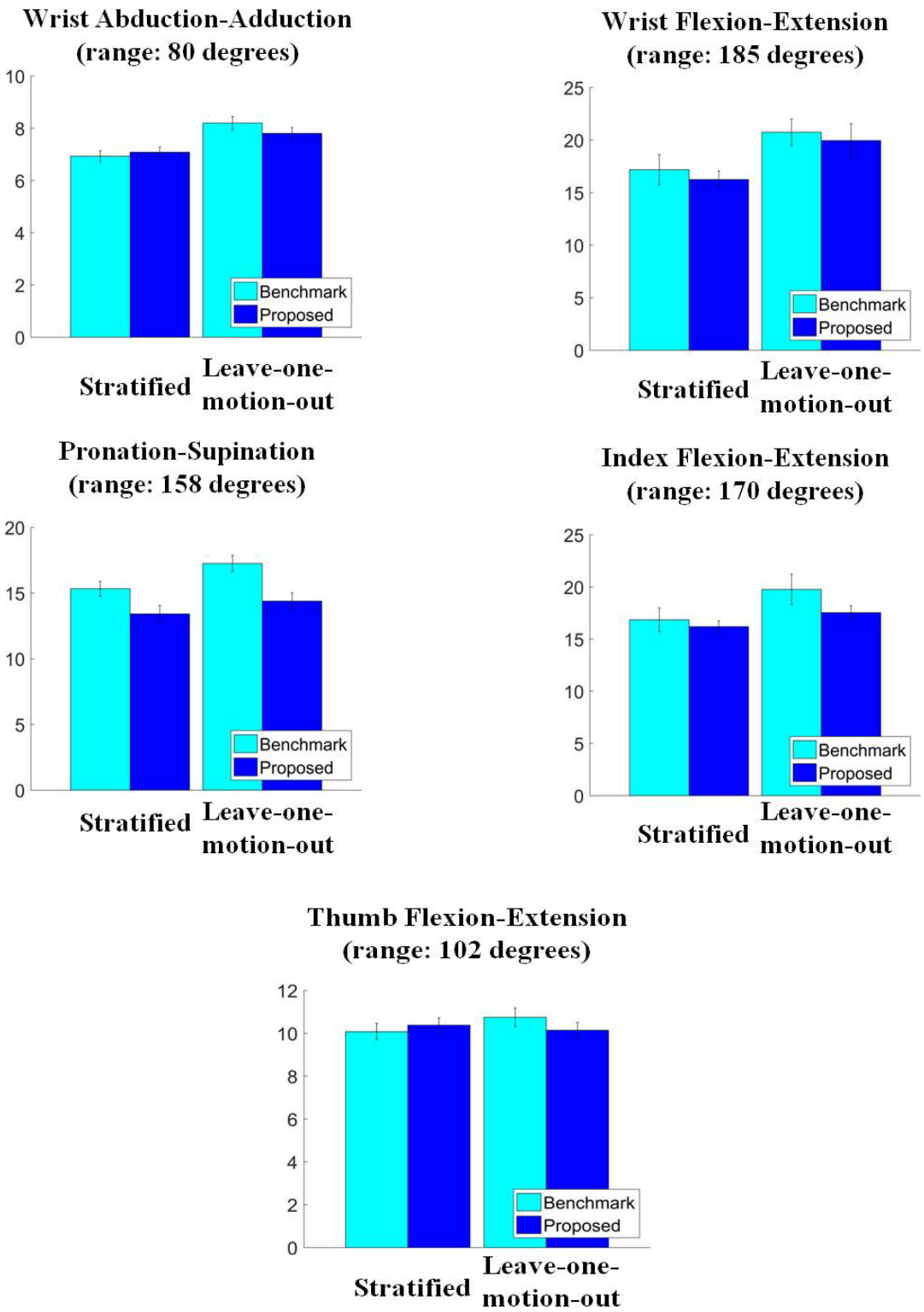


**Figure 6. Modeling results for five joint angles under two CV strategies.**

A hypothesis test was performed to test whether adding the simulated muscle features will significantly improve the prediction performance when the users are performing

unknown types of motions from the model training stage. The RMSE value for each sample can be obtained via Equation (7). For each type of angle, two vectors of the RMSEs can be calculated, where one is from the results of benchmark model the other is from the proposed model. A paired two-tiled t test was conducted on the two RMSE vectors for each joint angle. The null hypothesis is that the difference between the two RMSE vectors has the mean equal to zero, while the alternative hypothesis is that the mean is not zero. The normality assumption has been checked via histogram, in which the distribution of the differences between pairs follows the bell curve (Appendix D). The results of the hypothesis test for the stratified CV method and the leave-one-motion-out method are listed in Table 5.

**Table 5. P-values of the paired t-test for two CV strategies.**

| | **Wrist abd-add** | **Wrist flx-ext** | **Pro-sup** | **Index flx-ext** | **Thumb flx-ext** |
|---|---|---|---|---|---|
| **Stratified** | 0.120 | 0.190 | <0.001* | 0.465 | 0.148 |
| **Leave-one-motion-out** | 0.015* | 0.061 | <0.001* | 0.026* | 0.034* |

* P-value less than $\alpha = 0.05$.

According to Table 5, for the stratified CV strategy, significant differences were found in predicting the pronation-supination angles. Specifically, the proposed model performed significantly better than benchmark in the prediction of pronation-supination angles ($p < 0.001$) under the stratified CV strategy. Meanwhile, no significant differences were found in the prediction of the rest four joint angles (i.e., wrist abduction-adduction, wrist flexion-extension, index flexion-extension and thumb flexion-extension).

When applying leave-on-motion-out CV strategy, significant differences existed in predicting four types of angles. Specifically, the proposed method significantly outperforms the benchmark in the prediction of wrist abduction-adduction, pronation-supination, index flexion-extension and thumb flexion-extension angles with $p < 0.05$. However, the proposed model showed no significant advantage in the prediction of wrist flexion-extension angles ($p = 0.06$).

# CHAPTER 5
# DISCUSSION

## 5.1 Summary of Results

According to Figure 6 and Table 5, the proposed model performs significantly better than the benchmark model when dealing with new motion types. The prediction errors of 4 out of 5 type of angles ($p < 0.001$), namely, wrist abduction-adduction, pronation-supination, index flexion-extension and thumb flexion-extension angles, are significantly lower than benchmark. Although for the wrist flexion-extension angle, the average value of RMSEs for the proposed model is also lower than that of the benchmark model, no significant difference is found for the proposed one ($p = 0.06 > 0.05$). Therefore, we rejected the null hypothesis for the 4 out of 5 types of angles and concluded that adding the simulated muscle features will improve the prediction performance when performing unknown types of motions from the model training stage. When comparing the performance of the proposed model in terms of stratified and leave-one-motion-out CV strategies in Figure 6, their average RMSEs are close to each other. The encouraging results may indicate the robustness of proposed model to unknown types of motions. To validate the conjecture, paired Z-tests were applied to model coefficients fitted by different training data in order to quantify the robustness of the proposed model and the benchmark model in Section 5.2.

In terms of stratified CV methods, although the prediction error for the proposed method is lower than the benchmark for three types of angles, we failed to reject the hypothesis that the proposed model is significantly better than the benchmark, except for the prediction of pronation-supination angles. The insignificant advantage may be attributed to the information loss in the proposed two-stage modeling strategy. Namely, the sEMG signals (X) were firstly used to predict muscle features (ϒ), then the predicted muscle features were used to predict joint angles (Z). A two-stage modeling strategy may slightly reduce the performance since information losses will occur among the signals transformation (Kullback, 1959), including wavelet decomposition and MFPCA.

### 5.2 Robustness of Modeling Performance

To further justify the robustness of the proposed model, we compared the model coefficients fitted by different training data. This comparison was conducted on the benchmark model and the proposed model separately. The similarity of the normalized model coefficients was quantified using p-values (Clogg *et al.*, 1995; Paternoster *et al.*, 1998). The lower the p-values are, the less similar the model coefficients could be. This further reflects less stability of the model structure. Ten training sets were generated by selecting all the replications in the same type of motions each time. Accordingly, ten groups of coefficients were fitted for each type of motion based on those training sets. Afterwards, the similarity of the ten groups of model coefficients within each type of model was quantified based on the z-score (see Equation (10)), which follows a standard normal distribution with the null hypothesis of equality of the two model coefficients $\widehat{\boldsymbol{\beta}}_p$ and $\widehat{\boldsymbol{\beta}}_q$. This equation was proposed by Clogg (1995) and cited by Paternoster *et al.* (1998) assuming that the samples are independent and the coefficients are fitted from the same model with different sample sets.

$$\widehat{\boldsymbol{\vartheta}}_{p,q} = \frac{\widehat{\boldsymbol{\beta}}_p - \widehat{\boldsymbol{\beta}}_q}{\sqrt{s^2(\widehat{\boldsymbol{\beta}}_p) + s^2(\widehat{\boldsymbol{\beta}}_q)}}, \tag{10}$$

where $s^2(\widehat{\boldsymbol{\beta}})$ is the standard error of the regression coefficient $\boldsymbol{\beta}$; $p, q = 1, 2, \ldots, 10$; $\hat{\vartheta}_{p,q}$ is the paired z-score for evaluating the significance of difference between the coefficients $\widehat{\boldsymbol{\beta}}_p$ and $\widehat{\boldsymbol{\beta}}_q$. Afterwards, $\widehat{\boldsymbol{\vartheta}}_{p,q}$ was converted into p-value for comparison. Since multiple predictors were used, the averaged p-value was taken for each pair. Therefore, three matrices of averaged p-values were generated as presented in Figure 7 for a pair-wise comparison of coefficients of using X to predict ϒ, using ϒ to predict Z, and using X to predict Z, respectively. In Figure 7, each entry represents the significance of difference between two model coefficients. The matrices of p-values are available in Tables A4, A5 and A6 in Appendix C.

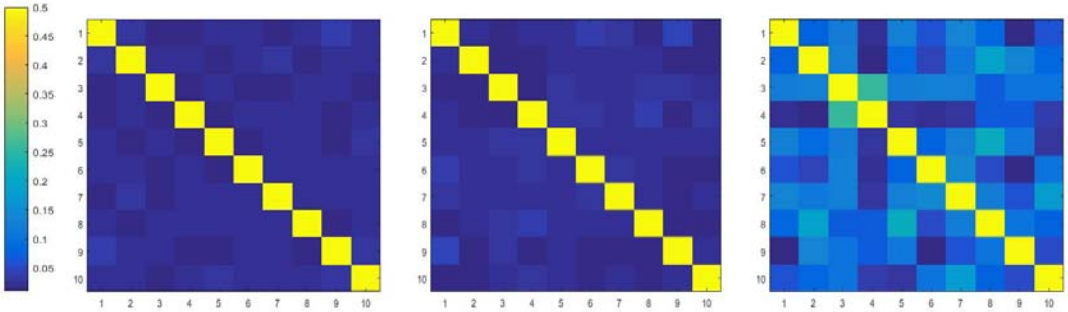

(a) (b) (c)

**Figure 7. Colored matrices for coefficients comparison (colored blocks represent averaged p-values.) (a) using X to predict Z, (b) using X to predict ϒ, and (c) using ϒ to predict Z.**

By comparing the p-value matrices in Figure 7, it can be concluded that the proposed model yields higher p-values in most entries. In other words, the proposed model is more robust to new motions than the benchmark model. Furthermore, the robustness of the proposed model may indicate that the performance of the proposed model is independent of the type of motions to some degree. The upper and lower bounds for the robustness of the proposed model may be determined by 1) the sensitivity of the adopted SVR to novelty, and 2) the applicable scope of the biomechanical model.

### 5.3 Comparison with Other Studies

Data-driven methods such as multiple linear regression and ANN have been used to predict continuous responses (joint angles or forces) of hand motions based on sEMG signals (Kitamura et al., 2006; Hioki et al., 2012). In our preliminary study, we also tried multiple linear regression model with lasso penalty on the data collected from subject 12. Because the residual plots for lasso regression (Figure A3 in Appendix D) indicated no non-linear relationship, we adopted SVR with linear kernal. The result showed that lasso performed worse than SVR in terms of the leave-one-motion-out strategy with an error of 9.20-22.50% while SVR provided a prediction error of 8.50-15.09% for the same set of data.

The prediction errors from our study are competitively low when comparing with those in other studies. For example, the mean absolute percentages of 11.62% for the thumb and

12.27% for the index finger were achieved in Smith's *et al.* (2008) study and the RMSE percentages of 7.1–11.8% for five finger joint angles were reported in a study conducted by Hioki *et al.* (2012). While in our study, the RMSE percentages were 8.67-11.63% for the five angles in the benchmark method and 8.49-10.78% for the proposed method (detailed percentages are in chapter 4). We also tried an ANN model with one hidden layer and 20 neurons as suggested by Mokhlesabadifarahani *et al.* (2015). The prediction errors are 9.21-21.77% for stratified CV strategy and 11.19-26.60% for leave-one-motion-out CV strategy when using sEMG to predict the five joint angles directly. In addition, although ANN models have been adopted in many studies of predicting finger joint angles because of their advantages in fitting relationship regardless of the linearity, their interpretability is an issue compared with statistical models (Intrator *et al.*, 2001). In our study, by adding muscle features, the interpretability of the model increases as each motion can be correlated to its activated muscle groups.

### 5.4. Limitations

Due to the better modeling performance and robustness, the proposed model has the potential to be applied to track human hand motions, especially for unknown types of motions. However, since the adopted biomechanical simulation model can only simulate five specific segments for fingers and wrist, the predicted angles are limited to the angles of wrist abduction-adduction, wrist flexion-extension, pronation-supination, index flexion-extension, and thumb flexion-extension. Other joint angles, such as the angles of middle finger flexion-extension, ring finger flexion-extension, and little thumb flexion-extension cannot be captured in the current model.

### 5.5. Conclusions and Future Works

This study provided a biomechanical knowledge-driven data fusion modeling strategy to integrate the biomechanical simulations and data-driven models. The modeling strategy achieved good performances in predicting joint angles of human hand motions especially for unknown types of motions. The proposed strategy showed advantages in prediction performance and robustness for unknown types of motions over the benchmark data-driven

model. Therefore, this model presents a novel and effective approach to integrate the computer simulations and the data-driven models in human factors and ergonomics.

In the future, the predicted joint angles will be further used to serve as the classification inputs to help distinguish different types of motions. A more flexible and informative biomechanical simulation model will be adopted to simulate the motions for more fingers on human hands, hence leading to more general usages of the proposed method. From the modeling perspective, more efficient models for important feature selection will be investigated to enhance the interpretability of the proposed model. As a generalization, the proposed data fusion strategy will be used in other human factors and ergonomics research domains (e.g., cognitive load quantification, occupational safety analysis, etc.).

## Appendix A. Calculation of Angles

The wrist flexion-extension angles were calculated via the angles between center line of defined hand plane and the surface normal of wrist. The plane of the hand was defined by marker handctr (6), handlt (6) and middleMCP (10). The surface normal of wrist was calculated from CMCd (2), ulnar (3), and CDCp (1). The abduction (adduction) angle was the angle between hand center line and the wrist axis. The wrist axis was defined by the vector between the two markers which were ulnar (3) and CMCd (2). The hand center line was the angle between the segment connected by Handctr (6) and middleMCP (10). Pronation (supination) angle was calculated from the relative angle between the wrist at the starting point and wrist axis at current frame. Index flexion angles were the one between the first segment of index finger and hand surface normal. It involved indexMCP (11) and indexDIP (20). Thumb flexion angle was the one between thumb and hand axis. It involved tmbMCP (5) and tmbDIP (12), and middleMCP (10) and middleDIP (19).

**Table A1. Name list of markers.**

| Code | Name | Code | Name |
|---|---|---|---|
| 1 | CMCd | 11 | indexPIP |
| 2 | ulnar | 12 | middleMCP |
| 3 | CMCp | 13 | middleDIP |
| 4 | handctr | 14 | middlePIP |
| 5 | handtmb | 15 | ringMCP |
| 6 | handlt | 16 | ringDIP |
| 7 | tmbMCP | 17 | ringPIP |
| 8 | tmbdDIP | 18 | littleMCP |
| 9 | indexMCP | 19 | littleDIP |
| 10 | indexDIP | 20 | littlePIP |

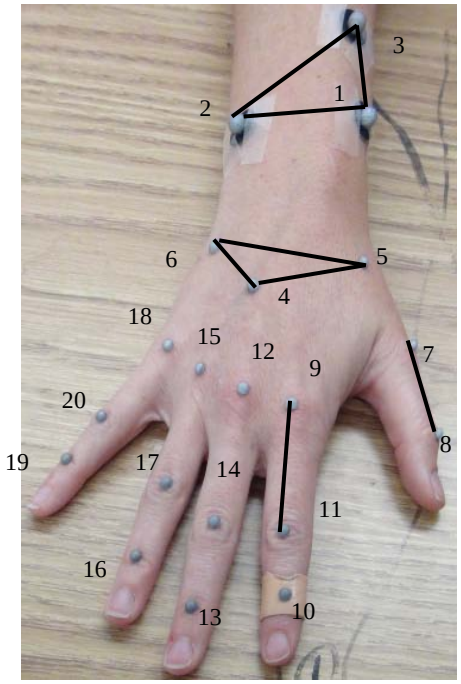


**Figure A1. Marker placement with labels.**

## Appendix B. Estimation of PC Scores

The following equations are calculated based on Happ's et al. (2016) study.

Let $Z_n^{(k)}, n = 1, 2, \ldots N,$ denotes the nth observation at the k-th joint angle where $k = 1, 2, \ldots, 5.$ $Z_n^{(k)}$ is a function of time. *N* is the sample size. Similarly, data from the muscle features can be denoted as $\gamma_1^{(h)}, \gamma_2^{(h)}, \ldots, \gamma_N^{(h)}$ where $h = 1, 2, \ldots, 60.$ We take $Z_n^{(k)}$ as an example to illustrate the estimation process.

Firstly, For each dimension $Z^{(k)}$, we estimated a univariate functional PC scores $\varepsilon_{n,m}^{(k)}$ and eigenfunctions $\phi_m^{(k)}$ where $m = 1,2, \ldots, M, k = 1,2, \ldots, p,$ (for $Z^{(k)}$, $p = 5$). *M* was the number of PCs extracted from the observation. We defined the matrix $\boldsymbol{A} \in \mathbb{R}^{N \times M_+}$, where each row was a concatenation of scores on each dimension $(\varepsilon_{n,1}^{(1)}, \ldots, \varepsilon_{n,M}^{(1)}, \ldots, \varepsilon_{n,1}^{(p)}, \ldots, \varepsilon_{n,M}^{(p)})$ for each observation. Then, an estimation for the block matrix $B \in \mathbb{R}^{M_+ \times M_+}$ was calculated based on Happ's *et al.* (2016) study where $\boldsymbol{B} = (N-1)^{-1}\boldsymbol{A}^T\boldsymbol{A}$. Next, we performed a matrix eigen analysis for $\boldsymbol{B}$ which provided us results in eigenvalues $\boldsymbol{v}_m$ and orthonormal eigenvectors $\boldsymbol{c}_m$. Finally, we had all the values to eatimate the multivariate eigenfunctions given by

$$\hat{\psi}_m^{(k)}(t) = \sum_{q=1}^{M} [\boldsymbol{c}_m]_q^{(k)} \phi_q^{(k)}(t),\ t = 1,2,..T.m = 1,2,\ldots,M, \tag{A.1}$$

and multivariate scores were given by

$$\hat{\rho}_{n,m} = \sum_{k=1}^{p} \sum_{q=1}^{M} [\boldsymbol{c}_m]_q^{(k)} \varepsilon_{n,q}^{(k)} = \boldsymbol{A}_n . \boldsymbol{c}_m. \tag{A.2}$$

After having PC scores and eigen-functions, we can reconstruct the estimated trajectories for the dimension $k$ $(k = 1,2, \ldots, p)$ of the sample $n$ via

$$\hat{Z}_n^{(k)} = \sum_{m=1}^{M} \hat{\rho}_{n,m} \hat{\psi}_m^{(k)}, \tag{A.3}$$

Note that each eigen-function $\psi_m^{(k)}$ had the same structure as $Z_n^{(k)}$. For each observation, we extracted 5 PCs from $Z_n^{(k)}$ and 7 PCs from $\gamma_n^{(h)}$ so that the PC scores could explain more than 90% of the variation for both types of data.

## Appendix C. Tables of Performance Measurements and Hypothesis Tests

**Table C1. Prediction results for stratified CV method.**

| | Model | k=1 | k=2 | k=3 | k=4 | k=5 |
|---|---|---|---|---|---|---|
| **Averaged** | X-Z | 6.93 | 17.19 | 15.33 | 16.85 | 10.08 |
| **RMSE** | X-Y-Z | 7.08 | 16.25 | 13.41 | 16.20 | 10.38 |
| **Standard** | X-Z | 0.20 | 1.42 | 0.56 | 1.13 | 0.38 |
| **Error** | X-Y-Z | 0.20 | 0.80 | 0.65 | 0.55 | 0.34 |

**Table C2. Prediction results for leave-one-motion-out CV method.**

| | Model | k=1 | k=2 | k=3 | k=4 | k=5 |
|---|---|---|---|---|---|---|
| **Averaged** | X-Z | 8.20 | 20.75 | 17.25 | 19.77 | 10.75 |
| **RMSE** | X-Y-Z | 7.80 | 19.95 | 14.39 | 17.54 | 10.14 |
| **Standard** | X-Z | 0.25 | 1.26 | 0.61 | 1.48 | 0.43 |
| **Error** | X-Y-Z | 0.23 | 1.60 | 0.63 | 0.67 | 0.35 |

**Table C3. Averaged p-values for using Y to predict Z.**

| Motion 1 | Motion 2 | Motion 3 | Motion 4 | Motion 5 | Motion 6 | Motion 7 | Motion 8 | Motion 9 | Motion 10 |
|---|---|---|---|---|---|---|---|---|---|
| 0.50 | 0.07 | 0.12 | 0.02 | 0.12 | 0.06 | 0.14 | 0.08 | 0.01 | 0.06 |
| 0.07 | 0.50 | 0.12 | 0.01 | 0.09 | 0.04 | 0.11 | 0.19 | 0.14 | 0.08 |
| 0.12 | 0.12 | 0.50 | 0.26 | 0.12 | 0.12 | 0.13 | 0.06 | 0.11 | 0.10 |
| 0.02 | 0.01 | 0.26 | 0.50 | 0.02 | 0.02 | 0.02 | 0.06 | 0.06 | 0.04 |
| 0.12 | 0.09 | 0.12 | 0.02 | 0.50 | 0.07 | 0.13 | 0.21 | 0.11 | 0.03 |
| 0.06 | 0.04 | 0.12 | 0.02 | 0.07 | 0.50 | 0.14 | 0.05 | 0.01 | 0.11 |
| 0.14 | 0.11 | 0.13 | 0.02 | 0.13 | 0.14 | 0.50 | 0.12 | 0.06 | 0.17 |
| 0.08 | 0.19 | 0.06 | 0.06 | 0.21 | 0.05 | 0.12 | 0.50 | 0.10 | 0.07 |
| 0.01 | 0.14 | 0.11 | 0.06 | 0.11 | 0.01 | 0.06 | 0.10 | 0.50 | 0.05 |
| 0.06 | 0.08 | 0.10 | 0.04 | 0.03 | 0.11 | 0.17 | 0.07 | 0.05 | 0.50 |

**Table C4. Averaged p-values for using X to predict Y.**

| Motion 1 | Motion 2 | Motion 3 | Motion 4 | Motion 5 | Motion 6 | Motion 7 | Motion 8 | Motion 9 | Motion 10 |
|---|---|---|---|---|---|---|---|---|---|
| 0.50 | 0.02 | 0.02 | 0.02 | 0.02 | 0.04 | 0.03 | 0.02 | 0.05 | 0.02 |
| 0.02 | 0.50 | 0.01 | 0.02 | 0.02 | 0.02 | 0.03 | 0.02 | 0.02 | 0.01 |
| 0.02 | 0.01 | 0.50 | 0.01 | 0.03 | 0.02 | 0.02 | 0.03 | 0.03 | 0.03 |
| 0.02 | 0.02 | 0.01 | 0.50 | 0.03 | 0.03 | 0.02 | 0.04 | 0.02 | 0.03 |
| 0.02 | 0.02 | 0.03 | 0.03 | 0.50 | 0.02 | 0.03 | 0.02 | 0.02 | 0.02 |
| 0.04 | 0.02 | 0.02 | 0.03 | 0.02 | 0.50 | 0.03 | 0.02 | 0.02 | 0.02 |
| 0.03 | 0.03 | 0.02 | 0.02 | 0.03 | 0.03 | 0.50 | 0.02 | 0.02 | 0.02 |
| 0.02 | 0.02 | 0.03 | 0.04 | 0.02 | 0.02 | 0.02 | 0.50 | 0.02 | 0.01 |
| 0.05 | 0.02 | 0.03 | 0.02 | 0.02 | 0.02 | 0.02 | 0.02 | 0.50 | 0.02 |
| 0.02 | 0.01 | 0.03 | 0.03 | 0.02 | 0.02 | 0.02 | 0.01 | 0.02 | 0.50 |

**Table C5. Averaged p-values for using X to predict Z.**

| Motion 1 | Motion 2 | Motion 3 | Motion 4 | Motion 5 | Motion 6 | Motion 7 | Motion 8 | Motion 9 | Motion 10 |
|---|---|---|---|---|---|---|---|---|---|
| 0.50 | 0.03 | 0.02 | 0.02 | 0.02 | 0.02 | 0.02 | 0.02 | 0.04 | 0.02 |
| 0.03 | 0.50 | 0.02 | 0.03 | 0.02 | 0.03 | 0.04 | 0.02 | 0.02 | 0.03 |
| 0.02 | 0.02 | 0.50 | 0.01 | 0.02 | 0.02 | 0.02 | 0.03 | 0.03 | 0.02 |
| 0.02 | 0.03 | 0.01 | 0.50 | 0.02 | 0.02 | 0.03 | 0.02 | 0.02 | 0.02 |
| 0.02 | 0.02 | 0.02 | 0.02 | 0.50 | 0.02 | 0.03 | 0.02 | 0.02 | 0.03 |
| 0.02 | 0.03 | 0.02 | 0.02 | 0.02 | 0.50 | 0.02 | 0.02 | 0.03 | 0.02 |
| 0.02 | 0.04 | 0.02 | 0.03 | 0.03 | 0.02 | 0.50 | 0.03 | 0.02 | 0.02 |
| 0.02 | 0.02 | 0.03 | 0.02 | 0.02 | 0.02 | 0.03 | 0.50 | 0.02 | 0.02 |
| 0.04 | 0.02 | 0.03 | 0.02 | 0.02 | 0.03 | 0.02 | 0.02 | 0.50 | 0.03 |
| 0.02 | 0.03 | 0.02 | 0.02 | 0.03 | 0.02 | 0.02 | 0.02 | 0.03 | 0.50 |

## Appendix D. Figures for Assumption Check

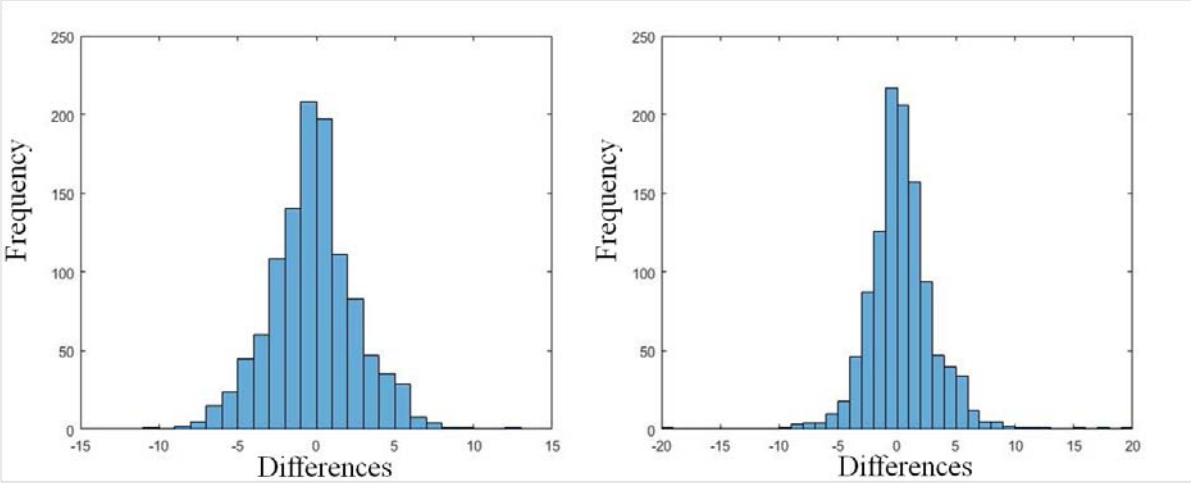


(a) (b)

**Figure D1. Histograms for normality assumption check for paired t-test (x axis refers to differences of RMSE between benchmark model and proposed model.) (a) using stratified CV strategy, (b) using leave-one-motion-out CV strategy.**

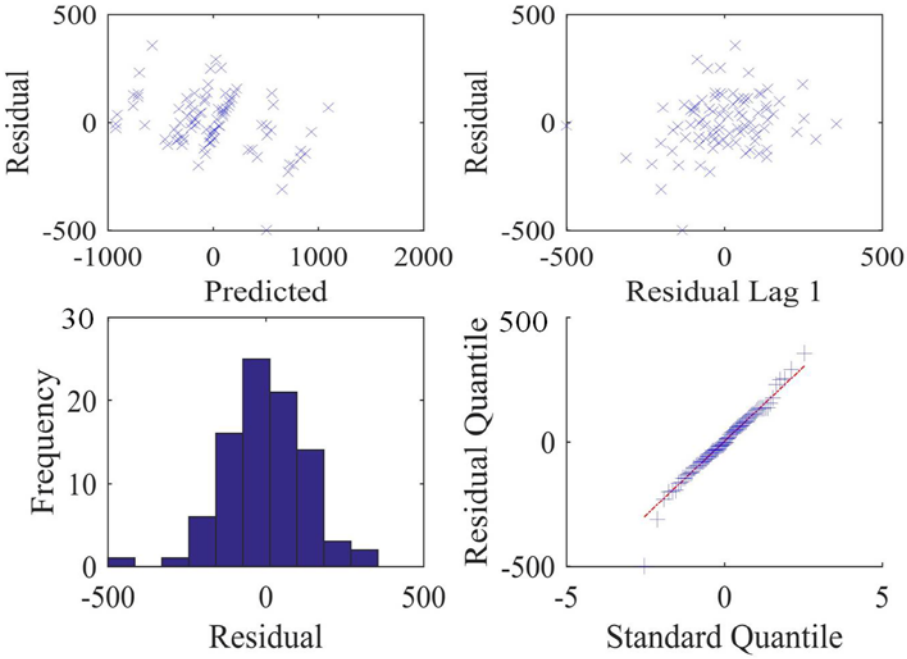


**Figure D2. Residual plots for multiple linear regression model.**

The upper left subplot shows the residual versus predicted value. The upper right

subplot represents the residual versus the residual for the next observation. The lower left subplot is the histogram of the residuals. And the last subplot is the quantile-quantile (Q-Q) plot.

**References**


Adewuyi, A. A., Hargrove, L. J., & Kuiken, T. A. (2016). An analysis of intrinsic and extrinsic hand muscle EMG for improved pattern recognition control. *IEEE Transactions on Neural Systems and Rehabilitation Engineering*, *24*(4), 485-494.

Akhlaghi, N., Baker, C. A., Lahlou, M., Zafar, H., Murthy, K. G., Rangwala, H. S., ... & Sikdar, S. (2016). Real-time classification of hand motions using ultrasound imaging of forearm muscles. *IEEE Transactions on Biomedical Engineering*, *63*(8), 1687-1698.

Al-Timemy, A. H., Bugmann, G., Escudero, J., & Outram, N. (2013). Classification of finger movements for the dexterous hand prosthesis control with surface electromyography. *IEEE Journal of Biomedical and Health Informatics*, *17*(3), 608-618.

Alazrai, R., Alabed, D., Alnuman, N., Khalifeh, A., & Mowafi, Y. (2016, December). sEMG-based approach for estimating wrist and fingers joint angles using discrete wavelet transform. In *Biomedical Engineering and Sciences (IECBES), 2016 IEEE EMBS Conference on* (pp. 596-599). IEEE.

Alkan, A., & Günay, M. (2012). Identification of EMG signals using discriminant analysis and SVM classifier. *Expert Systems with Applications*, *39*(1), 44-47.

Antfolk, C., Cipriani, C., Controzzi, M., Carrozza, M. C., Lundborg, G., Rosén, B., & Sebelius, F. (2010). Using EMG for real-time prediction of joint angles to control a prosthetic hand equipped with a sensory feedback system. *Journal of Medical and Biological Engineering*, *30*(6), 399-406.

Arnold, E. M., Hamner, S. R., Seth, A., Millard, M., & Delp, S. L. (2013). How muscle fiber lengths and velocities affect muscle force generation as humans walk and run at different speeds. *Journal of Experimental Biology*, *216*(11), 2150-2160.

Basak, D., Pal, S., & Patranabis, D. C. (2007). Support vector regression. *Neural Information Processing-Letters and Reviews*, *11*(10), 203-224.

Chu, J. U., Moon, I., & Mun, M. S. (2006). A real-time EMG pattern recognition system based on linear-nonlinear feature projection for a multifunction myoelectric hand. *IEEE Transactions on biomedical engineering*, *53*(11), 2232-2239.

Clogg, C. C., Petkova, E., & Haritou, A. (1995). Statistical methods for comparing regression coefficients between models. *American Journal of Sociology, 100*(5), 1261-1293.

Delp, S. L., Anderson, F. C., Arnold, A. S., Loan, P., Habib, A., John, C. T., ... & Thelen, D. G. (2007). OpenSim: open-source software to create and analyze dynamic simulations of movement. *IEEE transactions on biomedical engineering*, *54*(11), 1940-1950.

Donoho, D. L., & Johnstone, I. M. (1995). Adapting to unknown smoothness via wavelet shrinkage. *Journal of the american statistical association*, *90*(432), 1200-1224.

Erol, A., Bebis, G., Nicolescu, M., Boyle, R. D., & Twombly, X. (2005, June). A review on vision-based full DOF hand motion estimation. In *Computer Vision and Pattern Recognition-Workshops, 2005. CVPR Workshops. IEEE Computer Society Conference on* (pp. 75-75). IEEE.

Federolf, P. A. (2013). A novel approach to solve the “missing marker problem” in marker-based motion analysis that exploits the segment coordination patterns in multi-limb motion data. *PloS one*, *8*(10), e78689.

Fontana, J. M., & Chiu, A. W. (2014). Analysis of electrode shift effects on wavelet features embedded in a myoelectric pattern recognition system. *Assistive Technology*, *26*(2), 71-80.

Geisser, S. (1993). *Predictive inference* (Vol. 55). CRC press.

Goebl, W., & Palmer, C. (2013). Temporal control and hand movement efficiency in skilled music performance. *PloS one*, *8*(1), e50901.

Gonzalez, R. V., Buchanan, T. S., & Delp, S. L. (1997). How muscle architecture and moment arms affect wrist flexion-extension moments. *Journal of biomechanics*, *30*(7), 705-712.

Gregor, R. J., & Abelew, T. A. (1994). Tendon force measurements and movement control: a review. *Medicine and science in sports and exercise*, *26*(11), 1359-1372.

Happ, C., & Greven, S. (2016). Multivariate Functional Principal Component Analysis for Data Observed on Different (Dimensional) Domains. Journal of the American Statistical Association, (just-accepted).

Hioki, M., & Kawasaki, H. (2012). Estimation of finger joint angles from sEMG using a neural network including time delay factor and recurrent structure. *ISRN Rehabilitation*.

Holzbaur, K. R., Murray, W. M., & Delp, S. L. (2005). A model of the upper extremity for simulating musculoskeletal surgery and analyzing neuromuscular control. *Annals of*

*biomedical engineering*, *33*(6), 829-840.

Hsieh, C. J., Chang, K. W., Lin, C. J., Keerthi, S. S., & Sundararajan, S. (2008, July). A dual coordinate descent method for large-scale linear SVM. In *Proceedings of the 25th international conference on Machine learning* (pp. 408-415). ACM.

Ishii, C., Harada, A., Nakakuki, T., & Hashimoto, H. (2011, August). Control of myoelectric prosthetic hand based on surface emg. In *Mechatronics and Automation (ICMA), 2011 International Conference on* (pp. 761-766). IEEE.

Intrator, O., & Intrator, N. (2001). Interpreting neural-network results: a simulation study. *Computational statistics & data analysis*, *37*(3), 373-393.

Jiang, M. W., Wang, R. C., Wang, J. Z., & Jin, D. W. (2006, January). A method of recognizing finger motion using wavelet transform of surface EMG signal. In *Engineering in Medicine and Biology Society, 2005. IEEE-EMBS 2005. 27th Annual International Conference of the* (pp. 2672-2674). IEEE.

Kanitz, G. R., Antfolk, C., Cipriani, C., Sebelius, F., & Carrozza, M. C. (2011, August). Decoding of individuated finger movements using surface EMG and input optimization applying a genetic algorithm. In *Engineering in Medicine and Biology Society, EMBC, 2011 Annual International Conference of the IEEE* (pp. 1608-1611). IEEE.

Khushaba, R. N., Al-Ani, A., & Al-Jumaily, A. (2010). Orthogonal fuzzy neighborhood discriminant analysis for multifunction myoelectric hand control. *IEEE Transactions on Biomedical Engineering*, *57*(6), 1410-1419.

Kitamura, T., Tsujiuchi, N., & Koizumi, T. (2006, August). Hand motion estimation by EMG signals using linear multiple regression models. In *Engineering in Medicine and Biology Society, 2006. EMBS'06. 28th Annual International Conference of the IEEE* (pp. 1339-1342). IEEE.

Kullback, S. (1959). *Information theory and statistics*. John Wiley & Sons, New York.

Liu, J. (2014). Feature dimensionality reduction for myoelectric pattern recognition: A comparison study of feature selection and feature projection methods. *Medical engineering & physics*, *36*(12), 1716-1720.

Logar, G., & Munih, M. (2015). Estimation of Joint Forces and Moments for the In-Run and Take-Off in Ski Jumping Based on Measurements with Wearable Inertial

Sensors. *Sensors*, *15*(5), 11258-11276.

Lyons, G. M., Culhane, K. M., Hilton, D., Grace, P. A., & Lyons, D. (2005). A description of an accelerometer-based mobility monitoring technique. *Medical engineering & physics*, *27*(6), 497-504.

Ma, L., Chablat, D., Bennis, F., Zhang, W., & Guillaume, F. (2010). A new muscle fatigue and recovery model and its ergonomics application in human simulation. *Virtual and Physical Prototyping*, *5*(3), 123-137.

Ma, Y., Mao, Z. H., Jia, W., Li, C., Yang, J., & Sun, M. (2011). Magnetic hand tracking for human-computer interface. *IEEE Transactions on Magnetics*, *47*(5), 970-973.

Misiti, M., Misiti, Y., Oppenheim, G., & Poggi, J. M. (1996). Wavelet toolbox. *The MathWorks Inc., Natick, MA*, *15*, 21.

Mokhlesabadifarahani, B., & Gunjan, V. K. (2015). *EMG Signals Characterization in Three States of Contraction by Fuzzy Network and Feature Extraction*. Springer.

Murata, N., Yoshizawa, S., & Amari, S. I. (1994). Network information criterion-determining the number of hidden units for an artificial neural network model. *IEEE Transactions on Neural Networks*, *5*(6), 865-872.

Naik, G. R., Kumar, D. K., & Arjunan, S. (2009, September). Use of sEMG in identification of low level muscle activities: Features based on ICA and fractal dimension. In *Engineering in Medicine and Biology Society, 2009. EMBC 2009. Annual International Conference of the IEEE* (pp. 364-367). IEEE.

Najafi, B., Aminian, K., Paraschiv-Ionescu, A., Loew, F., Bula, C. J., & Robert, P. (2003). Ambulatory system for human motion analysis using a kinematic sensor: monitoring of daily physical activity in the elderly. *IEEE Transactions on biomedical Engineering*, *50*(6), 711-723.

Nazmi, N., Abdul Rahman, M. A., Yamamoto, S. I., Ahmad, S. A., Zamzuri, H., & Mazlan, S. A. (2016). A Review of Classification Techniques of EMG Signals during Isotonic and Isometric Contractions. *Sensors*, *16*(8), 1304.

Ngeo, J., Tamei, T., & Shibata, T. (2012). Continuous estimation of finger joint angles using muscle activation inputs from surface EMG signals. In *Engineering in Medicine and Biology Society (EMBC), 2012 Annual International Conference of the IEEE* (pp. 2756-2759). IEEE.

Noort, J. C., Kortier, H. G., van Beek, N., Veeger, D. H., & Veltink, P. H. (2016). Measuring 3D Hand and Finger Kinematics—A Comparison between Inertial Sensing and an Opto-Electronic Marker System. *PloS One*, *11*(11), e0164889.

Paternoster, R., Brame, R., Mazerolle, P., & Piquero, A. (1998). Using the correct statistical test for the equality of regression coefficients. *Criminology*, *36*(4), 859-866.

Patton, J. L. (1993). *Forward dynamic modeling of human locomotion* (Doctoral dissertation, Michigan State University).

Reis, L. P., Moreira, A. P., Lima, P. U., Montaño, L., & Muñoz-Martinez, V. (Eds.). (2015). *Robot 2015: Second Iberian Robotics Conference: Advances in Robotics* (Vol. 1). Springer.

Rheingold, H. (1991). *Virtual Reality: Exploring the Brave New Technologies*. Simon & Schuster Adult Publishing Group.

Robertson, G., Caldwell, G., Hamill, J., Kamen, G., & Whittlesey, S. (2013). *Research methods in biomechanics*, *2E*. Human Kinetics.

Seth, A., Sherman, M., Reinbolt, J. A., & Delp, S. L. (2011). OpenSim: a musculoskeletal modeling and simulation framework for in silico investigations and exchange. *Procedia Iutam*, *2*, 212-232.

Shrirao, N. A., Reddy, N. P., & Kosuri, D. R. (2009). Neural network committees for finger joint angle estimation from surface EMG signals. *Biomedical engineering online*, *8*(1), 2.

Simone, L. K., & Kamper, D. G. (2005). Design considerations for a wearable monitor to measure finger posture. *Journal of NeuroEngineering and Rehabilitation*, *2*(1), 5.

Smith, R. J., Tenore, F., Huberdeau, D., Etienne-Cummings, R., & Thakor, N. V. (2008, August). Continuous decoding of finger position from surface EMG signals for the control of powered prostheses. In *Engineering in Medicine and Biology Society, 2008. EMBS 2008. 30th Annual International Conference of the IEEE* (pp. 197-200). IEEE.

Sobahi, N. M. (2011). Denoising of EMG signals based on wavelet transform. *Asian Transactions on Engineering*, *1*(5), 17-23.

Tenore, F., Ramos, A., Fahmy, A., Acharya, S., Etienne-Cummings, R., & Thakor, N. V. (2007, August). Towards the control of individual fingers of a prosthetic hand using surface EMG signals. In *Engineering in Medicine and Biology Society, 2007. EMBS 2007. 29th*

*Annual International Conference of the IEEE* (pp. 6145-6148). IEEE.

Tenore, F. V., Ramos, A., Fahmy, A., Acharya, S., Etienne-Cummings, R., & Thakor, N. V. (2009). Decoding of individuated finger movements using surface electromyography. *IEEE transactions on biomedical engineering*, *56*(5), 1427-1434.

Tkach, D., Huang, H., & Kuiken, T. A. (2010). Study of stability of time-domain features for electromyographic pattern recognition. *Journal of neuroengineering and rehabilitation*, *7*(1), 21.

Tsang, W., Singh, K., & Fiume, E. (2005, July). Helping hand: an anatomically accurate inverse dynamics solution for unconstrained hand motion. In *Proceedings of the 2005 ACM SIGGRAPH/Eurographics symposium on Computer animation* (pp. 319-328). ACM.

Tyldesley, B. (1989). *Muscles, nerves & movement*.

Tyldesley, B., & Grieve, J. (2009). *Muscles, nerves and movement: in human occupation*. John Wiley & Sons.

Ueda, J., Gallagher, W., Moualeu, A., Shinohara, M., & Feigh, K. (2016). Adaptive Human-Robot Physical Interaction for Robot Coworkers. *Human Modeling for Bio-Inspired Robotics: Mechanical Engineering in Assistive Technologies*, 297.

US Department of Public Health Service (1992). Selected Topics in Surface Electromyography for Use in the Occupational Setting: Expert Perspectives.

Vapnik, V. (2013). *The nature of statistical learning theory*. Springer science & business media.

Vicon Motion Systems, *Vicon*, Oxford, England, https://www.vicon.com/.

Wu, J., Tian, Z., Sun, L., Estevez, L., & Jafari, R. (2015, June). Real-time American sign language recognition using wrist-worn motion and surface EMG sensors. In *Wearable and Implantable Body Sensor Networks (BSN), 2015 IEEE 12th International Conference on* (pp. 1-6). IEEE.

Xing, K., Yang, P., Huang, J., Wang, Y., & Zhu, Q. (2014). A real-time EMG pattern recognition method for virtual myoelectric hand control. *Neurocomputing*, *136*, 345-355.

Yan, J., Li, Y., Zheng, E., & Liu, Y. (2010). An accelerated human motion tracking system based on voxel reconstruction under complex environments. *Computer Vision–ACCV 2009*, 313-324.

Zardoshti-Kermani, M., Wheeler, B. C., Badie, K., & Hashemi, R. M. (1995). EMG feature evaluation for movement control of upper extremity prostheses. *IEEE Transactions on Rehabilitation Engineering*, *3*(4), 324-333.

Zhou, H., Hu, H., Harris, N. D., & Hammerton, J. (2006). Applications of wearable inertial sensors in estimation of upper limb movements. *Biomedical Signal Processing and Control*, *1*(1), 22-32.

Zhou, H., & Hu, H. (2008). Human motion tracking for rehabilitation—A survey. *Biomedical Signal Processing and Control*, *3*(1), 1-18.